Assessment of Avalanche Dynamics of the 2014 Everest Serac Fall Using GIS Hazard Mapping and RAMMS Simulation

Anish Dahal[1*], Khem Narayan Paudyal[2], Til Prasad Pangali Sharma[3], & Tanka Prasad Paudel[3]

[1]*M.Sc. in Mountain and Mountaineering Sciences, Nepal Mountain Academy, Tribhuvan University, Kathmandu*
[2]*Institute of Engineering, Pulchowk Campus, Tribhuvan University, Pulchowk, Lalitpur*
[3]*Nepal Mountain Academy, Ministry of Culture, Tourism and Civil Aviation, Nepal*
[*]*Corresponding Author: anish.msc@nepalmountain.edu.np*
DOI: http://doi.org/10.3126/jtha.v8i1.96399

Abstract

Avalanches pose a persistent and deadly hazard in high-mountain terrain, where steep topography, dynamic snowpack conditions, and rapid cryospheric change converge to generate extreme mass-movement events. The 2014 serac fall on the western shoulder of Mount Everest, which killed 16 Sherpa guides in the Khumbu Icefall, represents one of the most lethal single avalanche incidents recorded in Himalayan mountaineering history, yet its physical dynamics have not previously been analyzed through numerical simulation. This study presents an integrated assessment of avalanche hazards in the Upper Dudh Koshi Basin (Everest region, Nepal) by combining a GIS-based multi-criteria decision analysis (MCDA) using the Analytical Hierarchy Process (AHP) for regional susceptibility mapping with the Rapid Mass Movement Simulation (RAMMS) model for event-specific dynamic reconstruction. Seven terrain and climatic parameters, including slope, elevation, aspect, curvature, land cover, temperature, and precipitation, were derived from satellite and gridded climate datasets, reclassified into hazard levels, and combined through AHP-weighted overlay analysis to produce a five-class susceptibility map. The susceptibility mapping indicates that approximately 34% of the study area falls within the high to very high hazard categories, with the standard Everest climbing route traversing zones classified as very high risk throughout the Khumbu Icefall. RAMMS simulation of the 2014 event yielded a maximum flow height of approximately 35 m, a peak velocity of 36.2 m/s, and localized impact pressures exceeding 1,180 kPa. These modeled dynamics correspond closely with the spatial extent documented by post-event satellite imagery and with accounts from experienced mountaineers who validated the hazard map by independently locating observed avalanche source zones. The results illustrate the utility of this combined GIS-RAMMS framework for hazard assessment in data-scarce, high-alpine environments and suggest practical applications for route safety planning and evidence-based risk governance in Himalayan mountaineering.

Keywords: avalanche modelling, RAMMS, GIS, Himalaya, Everest, hazard mapping

Introduction

The Himalaya constitute one of the youngest and most tectonically active mountain belts on Earth, where ongoing orogenic uplift and accelerating cryospheric change produce a complex mosaic of natural hazards (Yadav et al., 2021; Owen, 2017). Among these hazards, snow and ice avalanches represent a persistent threat to lives, infrastructure, and livelihoods across mountain communities and the substantial population of seasonal workers engaged in high-altitude trekking and mountaineering (Eckert & Giacona, 2022). High Mountain Asia (HMA) supports the largest non-polar cryospheric system on Earth, sustaining river systems on which more than 1.9 billion people depend; this same system, however, generates a disproportionate burden of geohazards (Wester et al., 2019). Although glacial lake outburst floods have attracted considerable research attention in recent decades, avalanche events account for a substantial share of HMA fatalities, with Nepal alone recording 508 deaths between 1972 and 2022, predominantly among guides and high-altitude workers concentrated in the most hazardous terrain (Acharya et al., 2023).

The mechanisms governing Himalayan avalanche activity are diverse and spatially variable. Heavy snowfall combined with wind loading is a principal trigger on steep, north-facing slopes, where shading promotes the development of persistent weak layers within the snowpack (Hao et al., 2018). Rapid warming events during spring and summer months destabilize snowpacks through melt-freeze cycling, promoting wet slab release (Yanlong & Maohuan, 1986). In glaciated terrain, ice avalanches initiated by serac detachment represent a distinct and particularly hazardous mode of failure, characterized by high ice densities, long runout distances, and impact pressures that far exceed those of snow avalanches (Faillettaz et al., 2015; Kargel et al., 2016). The progressive warming of the Himalayan cryosphere is expected to increase the frequency of both wet snow avalanches and ice-related mass movements by destabilizing glacial ice and reducing permafrost cohesion, making quantitative hazard assessment increasingly urgent (Ballesteros-Canovas et al., 2018).

On 18 April 2014, a serac detached from the western shoulder of Mount Everest at approximately 6:30 AM local time and triggered a large ice avalanche that swept through the Khumbu Icefall. The event killed 16 Sherpa guides who were ferrying loads between Base Camp and Camp I, making it one of the deadliest avalanche incidents ever recorded in the Nepal Himalaya (Mehta & Raina, 2021). The serac block, estimated at approximately 41 m long, 22 m wide, and 34 m deep, detached from a hanging glacier on the western shoulder at an elevation of approximately 5,945 m and descended into the heavily trafficked corridor below. Despite the scale and consequences of the event, a detailed numerical reconstruction of its dynamics has not, to our knowledge, been undertaken, leaving a significant gap in the quantitative understanding of serac-fall mechanics in this setting.

The application of Geographic Information Systems (GIS) and physically-based numerical simulation to avalanche hazard assessment is well established in European and other mountain contexts (Christen et al., 2010; Buhler et al., 2013), and recent studies have demonstrated the potential of such methods in the Himalayan context (Thayyen et al., 2022; Yadav et al., 2023). However, the combination of GIS-based susceptibility mapping with event-specific simulation for a documented historical event in the Everest region remains an underexplored application. The extreme terrain, limited in-situ observational data, and restricted access to very high-resolution topographic products in the Nepal Himalaya present methodological challenges that must be addressed explicitly.

This study addresses these gaps through two complementary analyses. First, a GIS-based MCDA using the Analytical Hierarchy Process (AHP) is applied to produce a regional avalanche susceptibility map of the Upper Dudh Koshi Basin, integrating seven terrain and climatic parameters derived from freely available satellite and gridded climate products. Second, the RAMMS avalanche module is used to reconstruct the flow dynamics of the 2014 serac fall event, yielding spatially distributed outputs for flow height, velocity, impact pressure, momentum, and shear stress. The study then evaluates both products against historical event data and expert testimony from experienced mountaineers.

The specific research questions addressed are:

- Which areas of the Everest region exhibit the highest susceptibility to avalanche initiation and propagation, and does the standard climbing route traverse these zones?
- What were the principal dynamic characteristics of the 2014 serac fall, and do the modeled outputs correspond with documented observations of the event?
- How well does the combined GIS-RAMMS framework perform as a tool for avalanche hazard assessment in a data-scarce, high-alpine environment?

Study Area

The study area encompasses the Upper Dudh Koshi River Basin in the Mahalangur Himal subrange of Solukhumbu District, eastern Nepal (Figure 1). The basin extends from approximately 27°22' to 28°02' N and 86°24' to 87°02' E, covering roughly 1,651 km^2, and includes Mount Everest (8,849 m), Lhotse (8,516 m), and several other peaks exceeding 8,000 m. Relief across the basin exceeds 8,000 m over a horizontal distance of fewer than 30 km, producing slope gradients that commonly range between 30 and 55 degrees in the glaciated upper valleys. These gradients fall within the primary threshold range for avalanche initiation, which is typically cited as 28 to 55 degrees (McClung & Schaerer, 2006; Sharma & Ganju, 2000).

The Khumbu Glacier drains the southwestern flanks of Everest and Nuptse and is flanked throughout its upper reach by seracs and icefalls, of which the Khumbu Icefall is the most prominent. Stretching between approximately 5,400 and 7,000 m elevation, the Icefall forms a structurally unstable icescape of tilted slab seracs, open crevasse fields, and steep ice walls. It constitutes the mandatory passage on the standard South Col route and is traversed multiple times each season by guides, climbers, and high-altitude workers. The 2014 serac detachment occurred near the upper left margin of the Icefall at approximately 5,945 m (27.9953 N, 86.8788 E), within a zone of hanging glaciers on the western shoulder.

Climatically, the region is subject to a pronounced summer monsoon from June to September, during which the majority of annual precipitation falls; annual totals range from approximately 258 mm in high-elevation rain-shadow areas near the Tibetan border to over 2,500 mm in the lower southern valleys. Mean annual temperatures range from approximately 18 degrees Celsius at the valley floor to below negative 18 degrees Celsius on the highest ridges and summits. North-facing slopes above 5,000 m maintain persistent snowpack through much of the year, creating conditions conducive to both dry and wet slab avalanche activity depending on season. The combination of extreme relief, abundant snowfall, abundant serac-laden glacier margins, and dense seasonal use by climbers makes this basin an appropriate study area for integrated avalanche hazard assessment.

Figure 1

Study area location.

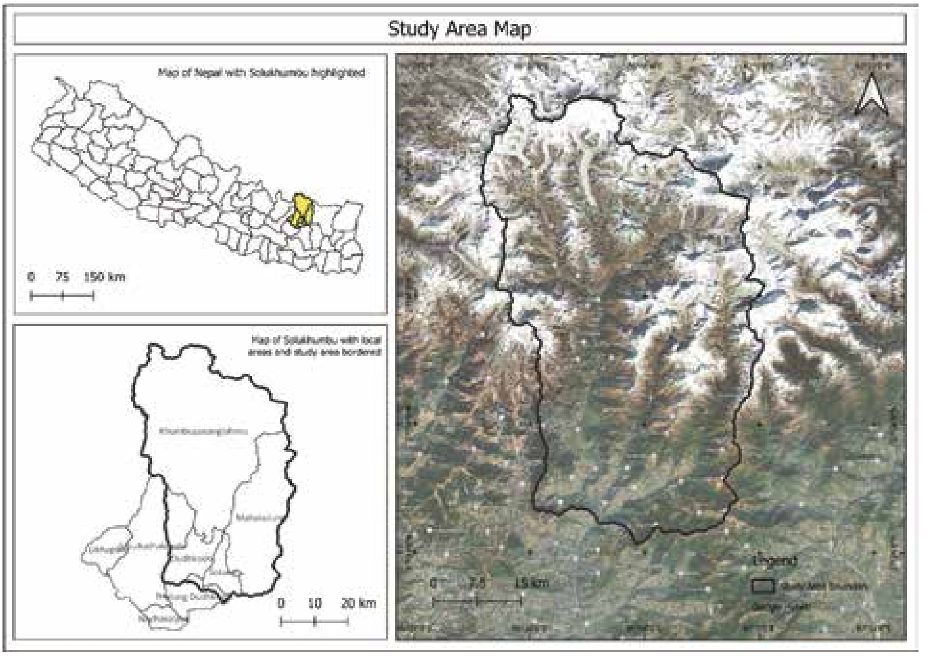

Note: Left inset: position of Solukhumbu District within Nepal.

Centre inset: municipal boundaries within the district, with study area outlined.

Right panel: Google Earth satellite image of the study area overlaid with the boundary polygon in QGIS (EPSG: 32645; 1:450,000 scale).

Materials and Methods

Data Sources

The analysis integrated topographic, land cover, and climatic datasets, all processed to a common spatial resolution of 10 m (Table 1). The primary terrain dataset was the ALOS PALSAR Digital Elevation Model (DEM), acquired from the Japan Aerospace Exploration Agency at a native resolution of 12.5 m. This product was chosen because it captures surface relief rather than canopy height, is freely available at a sub-30 m resolution for the Himalayan region, and has been used in several comparable Himalayan avalanche and geomorphological studies (Thayyen et al., 2022; Gilany & Iqbal, 2019). Land cover data were obtained from the ESRI Sentinel-2 Global Land Cover Explorer at 10 m resolution, a classification product based on Sentinel-2 spectral data that provides reliable discrimination of snow cover, glacial ice, and bare rock at high elevations.

Gridded climate data (temperature and precipitation) were obtained from WorldClim version 2.1 (Fick & Hijmans, 2017) at a native resolution of approximately 1 km^2, representing long-term monthly averages for the period 1970 to 2000.

WorldClim 2.1 was selected because it is the highest-resolution freely available global climate dataset covering this region and is routinely applied in Himalayan natural hazard susceptibility studies (Chaulagain et al., 2024; Sethia et al., 2018; Yadav et al., 2023). The dataset was produced by interpolating monthly observations from between 9,000 and 60,000 weather stations using thin-plate smoothing splines with MODIS-derived land surface temperature, cloud cover, and elevation as covariates (Fick & Hijmans, 2017), incorporating data from a higher number of high-elevation stations than its predecessor version. It is acknowledged, however, that the 1 km resolution of the climatic inputs is coarser than the topographic datasets and that orographic precipitation gradients at the sub-kilometre scale are unlikely to be fully resolved; consequently, the climatic layers were assigned lower AHP weights than terrain factors. In-situ climate records for this elevation range are extremely sparse in the Nepal Himalaya, and no comparable freely available alternative dataset provides the spatial coverage and resolution required for this analysis.

Table 1

Data types, sources, and native spatial resolutions used in this study.

Data Type	Source	Native Resolution
DEM	ALOS PALSAR (JAXA)	12.5 m
Slope, Elevation, Aspect, Curvature	Derived from DEM	12.5 m
Land Cover	ESRI Global Land Cover (Sentinel-2)	10 m
Temperature	WorldClim 2.1 (Fick & Hijmans, 2017)	~1 km (30 arc-sec)
Precipitation	WorldClim 2.1 (Fick & Hijmans, 2017)	~1 km (30 arc-sec)

Note. All layers were resampled to a uniform spatial resolution of 10 m using bilinear interpolation prior to weighted overlay analysis. The temporal range of WorldClim 2.1 (1970-2000) captures the pre-warming baseline climate of the study area.

GIS-Based Avalanche Susceptibility Mapping

Avalanche susceptibility mapping was conducted using a GIS-based MCDA framework in QGIS 3.40.8. Seven parameters were selected based on their established relevance to avalanche initiation and propagation in Himalayan literature (Table 2): slope angle, elevation, aspect, profile curvature, land cover, mean annual temperature, and mean annual precipitation. Each continuous raster layer was reclassified into discrete susceptibility scores (0.1 to 5) based on thresholds drawn from peer-reviewed literature (Table 2). Scores were then combined using a weighted overlay approach in which each layer was multiplied by its AHP-derived weight and the resulting products summed to produce a composite avalanche susceptibility index.

Table 2

GIS parameter reclassification thresholds and susceptibility scores, with literature basis.

Parameter	Threshold / Class	Score	Key References
Slope	0-25 deg; 25-45 deg (max.); 45-60 deg; >60 deg	0.1; 5; 3; 1	McClung & Schaerer (2006); Sharma & Ganju (2000)
Elevation (m)	<4,000 m; 4,000-5,000 m; 5,000-7,000 m (max.); >7,000 m	Not scored; 0.1; 5; 3	Sharma & Ganju (2000)

Aspect	N/NE (337.5-67.5 deg, max.); E/SE (67.5-157.5 deg); S-W (157.5-337.5 deg)	5; 1; 0.1	Sharma & Ganju (2000); Kumar et al. (2016)
Profile Curvature	Convex (<0, max.); Planar (~0); Concave (>0)	5; 1; 0.1	Yilmaz (2016)
Land Cover	Snow (max.); Glacier; Bare rock	5; 1; 0.1	Ciolli et al. (1998); Snehmani et al. (2014)
Temperature (deg C)	-18 to -10 and 0 to 5 (max.); -10 to 0; >5	5; 3; 0.1	Strapazzon et al. (2021); Souckovd et al. (2022)
Precipitation (mm/yr)	0-350; 350-800; 800-1,500; 1,500-2,400 (max.)	1; 2; 3; 4	Ortner et al. (2024)

AHP Weight Derivation

Weights for each parameter were derived using the Analytical Hierarchy Process (AHP), a structured MCDA technique in which each criterion is compared pairwise against every other criterion using a numerical scale (Saaty, 1980). The pairwise comparison matrix (Table 3) was constructed based on a synthesis of Himalayan avalanche literature, with slope assigned the highest importance because slope angle is the primary physical determinant of shear stress on the snowpack. Elevation was ranked second, as it governs snowpack persistence and temperature regime. Aspect and curvature followed as secondary morphological controls. Land cover, temperature, and precipitation were assigned lower priorities, reflecting their role as modulating rather than primary triggering factors.

The consistency of the judgments was assessed through the Consistency Ratio (CR). The calculated CR of 0.094 is below the commonly accepted threshold of 0.10, indicating that the pairwise comparisons are sufficiently consistent for use in weighted overlay analysis (Saaty, 1980).

Table 3

AHP pairwise comparison matrix and resulting normalized weights.

Parameter	Slope	Elev.	Aspect	Curv.	Land Cov.	Temp.	Precip.	Weight (%)
Slope	1	4	6	7	8	8	8	44.9
Elevation	0.25	1	5	6	7	8	8	27.1
Aspect	0.17	0.20	1	3	4	5	5	11.4
Curvature	0.14	0.17	0.33	1	3	4	4	7.1
Land Cover	0.13	0.14	0.25	0.33	1	3	3	4.4
Temperature	0.13	0.13	0.20	0.25	0.33	1	1	2.5
Precipitation	0.13	0.13	0.20	0.25	0.33	1	1	2.5

Note. Consistency Ratio (CR) = 0.094 < 0.10, indicating acceptable consistency. Weights are normalized from the principal eigenvector of the decision matrix (lambda-max = 7.752).

The final composite susceptibility index was classified into five equal-interval risk zones using natural breaks classification in QGIS: Very Low (1), Low (2), Moderate (3), High (4), and Very High (5). These zones correspond to the following susceptibility index ranges: Very Low (0 to 111.7), Low (111.7 to 206.1), Moderate (206.1 to 300.6), High (300.6 to

395.1), and Very High (395.1 to 500) (Table 4).

Table 4

Susceptibility classification scheme, index ranges, areal extent, and proportional coverage.

Hazard Zone	Index Range	Area (km^2)	Proportion of Study Area (%)
Very Low	0-111.7	246.98	14.96
Low	111.7-206.1	386.07	23.39
Moderate	206.1-300.6	454.80	27.55
High	300.6-395.1	310.84	18.83
Very High	395.1-500	252.21	15.28

RAMMS Avalanche Simulation

The 2014 serac fall was reconstructed using RAMMS version 1.8.27 (Rapid Mass Movement Simulation; Christen et al., 2010). RAMMS implements the Voellmy-Salm (VS) friction model, which characterizes avalanche flow resistance through two empirical parameters: a dry-Coulomb friction coefficient (mu, representing basal friction at low velocities) and a turbulent drag coefficient (xi, dominating at high velocities). The model also incorporates a Random Kinetic Energy (RKE) sub-model to account for flow fluctuations. RAMMS has been extensively validated for dense-flow avalanches and serac-fall events in comparable high-mountain settings, including the 2012 Gyari avalanche in the Shyok Basin (Gilany & Iqbal, 2019) and multiple events in the Rishiganga-Raunthigad basin of the Indian Himalaya (Thayyen et al., 2022).

Input Parameters

The terrain foundation for the simulation was the 10 m resampled ALOS PALSAR DEM, which was used without further topographic modification. The release zone was defined by digitizing a polygon corresponding to the collapsed serac block, using pre- and post-event satellite imagery (McMillan, 2014; Jenkins, 2014) and the National Geographic analysis of the avalanche path as geometric references. The fracture depth (d0) was set to 35 m, consistent with published estimates for this specific event (McMillan, 2014) and falling within the typical range for a 10-year return-period event in this zone. A constant ice density of 900 kg m-3 was specified, appropriate for the cohesive glacial ice constituting the serac block. The return period was set to 10 years, reflecting repeated documentation of significant serac activity at this location.

Friction parameters mu and xi were calibrated following the RAMMS user manual for high-mountain terrain, using two altitude thresholds: tree line at 4,000 m and snow line at 5,000 m. Separate parameter sets were assigned for open-slope, channelled, gully, and flat terrain types to reflect the varied roughness along the avalanche path (Table 5). These values fall within the ranges reported for ice-dominated avalanches in comparable settings (Gilany & Iqbal, 2019; Christen et al., 2010).

Table 5

Voellmy-Salm friction parameters used in the RAMMS simulation, stratified by terrain type and altitude zone.

Terrain Type	mu (<4,000 m)	mu (4,000-5,000 m)	mu (>5,000 m)	xi range (m/s^2)
Open slope	0.260	0.240	0.225	1,750-2,500
Channelled	0.310	0.295	0.280	1,350-1,750
Gully	0.390	0.360	0.350	1,100-1,350
Flat	0.240	0.220	0.200	2,500-3,250

Note. Parameters follow the RAMMS user manual recommendations for terrain above the snow line, using altitude_limit_1 = 3,000 m and altitude_limit_2 = 5,000 m. Three values are provided for each mu parameter in the format [below 5,000 m] / [5,000 to 3,000 m] / [above 3,000 m].

The simulation was run for 300 seconds with a 2-second output dump interval and a momentum-based stopping criterion of 5%. Curvature correction was enabled to account for centripetal effects in the steeply curved Icefall terrain. The estimated release volume was 23,711 m^3, corresponding to the digitized serac polygon at a fracture depth of 35 m.

Uncertainty Considerations

Several sources of uncertainty are inherent to this simulation. First, the 12.5 m native DEM resolution means that sub-grid-scale terrain features, including narrow crevasse channels and individual serac margins, are not fully resolved, which may affect modeled flow dispersion and runout geometry. Second, the Voellmy-Salm friction parameters were calibrated from regional literature rather than from an independent set of observed runout data for this specific event, introducing parameter uncertainty. Third, the release volume was estimated from satellite imagery analysis and may differ from the actual detached mass. Fourth, the temporal climate baseline used for susceptibility mapping (1970 to 2000) pre-dates the 2014 event by several decades; given ongoing climate change, current snowpack and glaciological conditions may differ from those represented by the WorldClim 2.1 climatology.

Validation Strategy

Model outputs were evaluated through three complementary approaches. First, the spatial extent and trajectory of the RAMMS simulation were compared qualitatively with the post-event avalanche flow path documented by National Geographic (Jenkins, 2014) and with satellite imagery acquired on 26 April 2014, eight days after the event. Second, the susceptibility map was evaluated by overlaying the mapped locations of the 2014 fatalities, which were georeferenced from published accounts (Mehta and Raina, 2021), onto the hazard classification. Third, fourteen experienced mountaineers who had made multiple ascents of Everest were interviewed and asked to locate, on a Google Earth display, the positions of avalanches they had personally observed during their expeditions. These sightings were subsequently overlaid on the susceptibility map to assess the agreement between modeled hazard zones and empirical observations.

Results

Regional Avalanche Susceptibility Map

The weighted overlay of seven reclassified parameter layers produced the avalanche susceptibility map shown in Figure 2. The map exhibits a distinct altitudinal and topographic gradient. Very Low and Low risk zones are broadly concentrated in the lower-elevation valleys and on the more gradual terrain south of the main Himalayan crest, particularly in the Namche Bazaar area and along the Dudh Koshi valley floor. Moderate risk zones form a transitional band across mid-elevation terrain. High and Very High risk zones dominate the upper basin, corresponding to the steep glaciated flanks and cirque headwalls of the major peaks.

In areal terms, the Moderate risk zone is the largest single category (454.80 km^2; 27.6% of the study area), followed by Low (386.07 km^2; 23.4%), High (310.84 km^2; 18.8%), Very Low (246.98 km^2; 15.0%), and Very High (252.21 km^2; 15.3%). The High and Very High categories together account for 34.1% of the study area, indicating that approximately one-third of this high-altitude basin is characterized by terrain conditions broadly conducive to avalanche generation. The geographic concentration of these zones in the immediate surroundings of the Everest massif and the Khumbu Icefall corridor is the most operationally significant finding.

Figure 2

GIS-derived avalanche susceptibility map of the Upper Dudh Koshi Basin, Everest region.

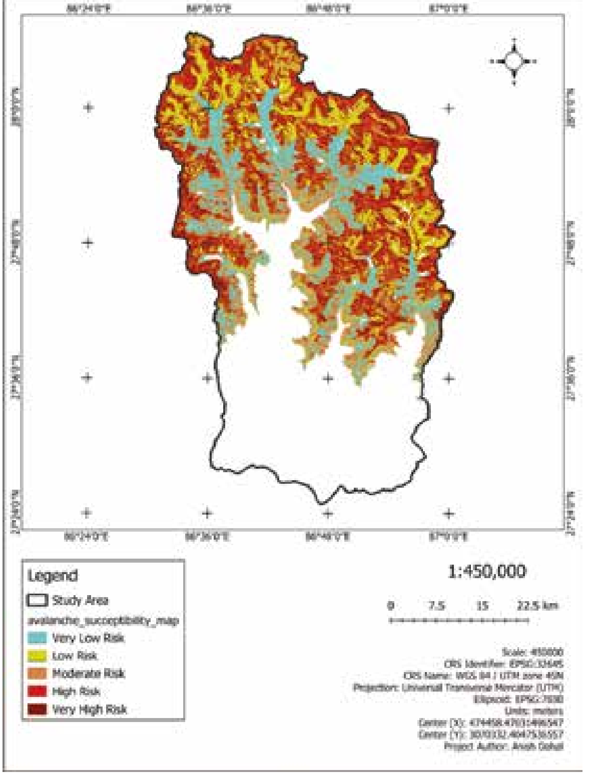

Note: Five hazard classes are shown: Very Low (cyan), Low (yellow-green), Moderate (brown), High (red), and Very High (dark red). Area statistics are provided in Table 4.

Scale 1:450,000; CRS: WGS 84 / UTM Zone 45N (EPSG 32645); projection: Universal Transverse Mercator.

Hazard Exposure along the Standard Climbing Route

Figure 3 presents a detailed view of the Everest massif, overlaying the standard South Col climbing route on the susceptibility map. The analysis reveals that the majority of the route between Base Camp and Camp II traverses terrain classified as High or Very High risk. In particular, the entire passage through the Khumbu Icefall falls within the Very High risk zone. This confirms, with quantitative spatial data, the well-known qualitative observation that the Icefall represents the most objectively hazardous section of the standard Everest ascent. Only brief sections of the route, primarily on the fixed glacier plateaus immediately above Camp I and in the upper Western Cwm, pass through Moderate or Low risk terrain.

Figure 3

Avalanche susceptibility map highlighting the Everest massif and the standard South Col climbing route (white line).

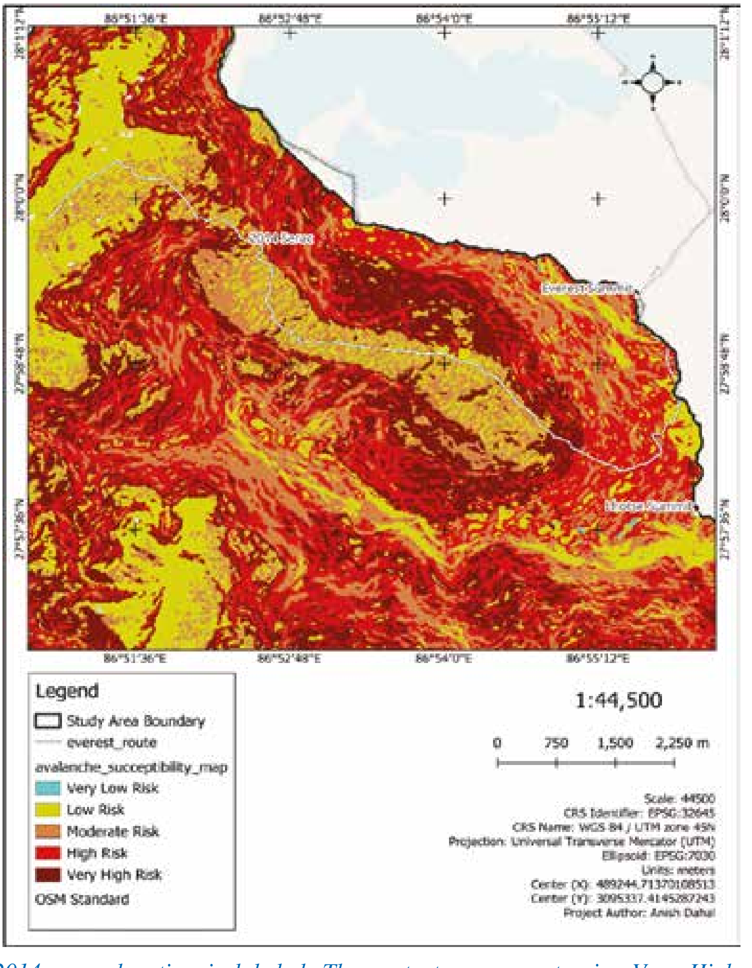

Note: The 2014 serac location is labeled. The route traverses extensive Very High risk terrain throughout the Khumbu Icefall.

Scale 1:44,500; same CRS and projection as Figure 2.

Susceptibility Map Validation

Spatial Correspondence with the 2014 Event

Figure 4 shows the 2014 serac trigger zone and the recorded fatality locations overlaid on the susceptibility map at 1:5,000 scale. The serac polygon is situated squarely within the Very High risk zone. Of the 14 recorded fatality locations, 11 fall within the Very High risk category and 2 within the High risk category. Only one fatality location is within the boundary between Moderate and High risk zones, likely reflecting the rapid runout of the dense ice mass beyond the highest-susceptibility terrain.

Figure 4

Avalanche susceptibility map at 1:5,000 scale, showing the Khumbu Icefall, the digitized 2014 serac trigger zone (white polygon, upper right), and georeferenced fatality locations (black points).

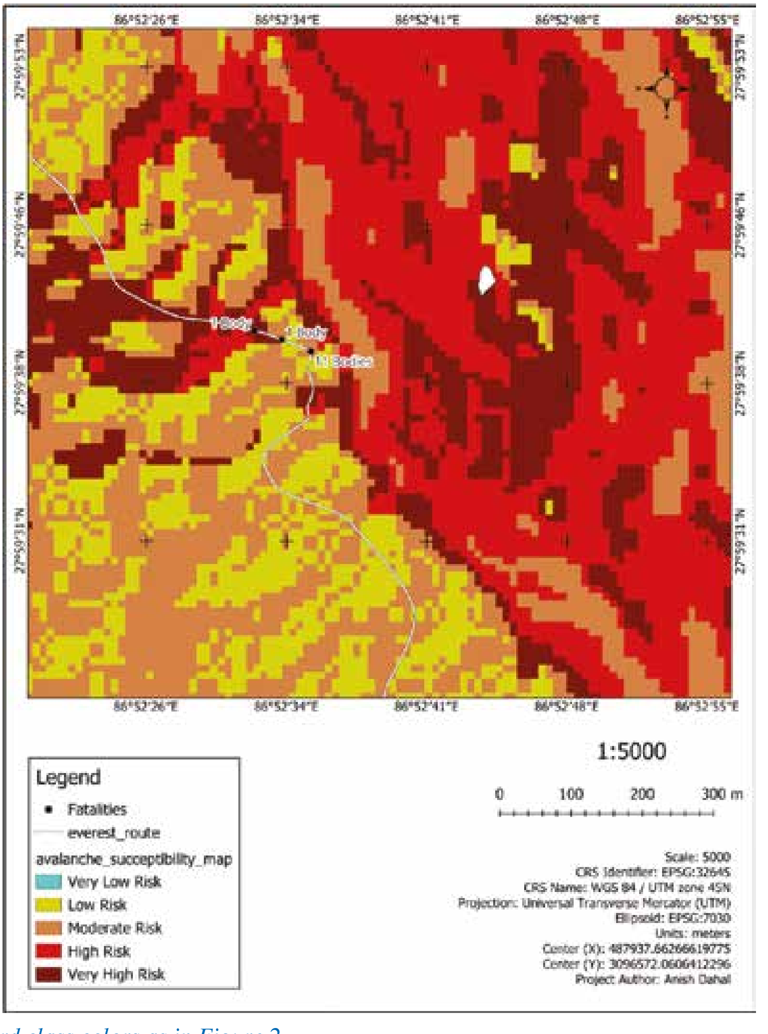

Note: Hazard class colors as in Figure 2.

Scale 1:5,000; same CRS and projection as Figure 2.

Expert-based Validation

Figure 5 presents the results of the mountaineer validation exercise. Of the 14 avalanche source locations independently identified by the experienced mountaineers, 8 (57.1%) fell within the Very High risk zone, 4 (28.6%) within the High risk zone, and 2 (14.3%) within the Moderate risk zone. In aggregate, 85.7% of the expert-identified source points correspond to the two highest susceptibility categories. This degree of agreement between the model output and firsthand field observations is consistent with the validation results reported in comparable AHP-based Himalayan studies, where high-risk zones typically capture 75 to 90% of documented events (Thayyen et al., 2022; Yadav et al., 2023). It should be noted that this validation is qualitative in nature and relies on recall rather than a systematic georeferenced inventory, which represents a limitation discussed further in Section 5.

Figure 5

Expert validation of the avalanche susceptibility map.

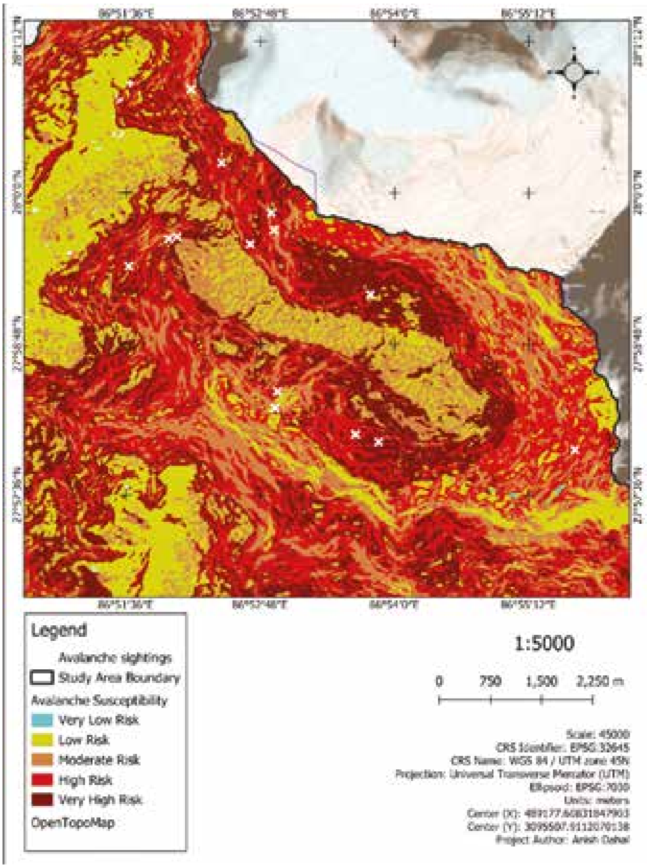

Note: White crosses indicate the 14 avalanche source locations independently identified by experienced mountaineers, overlaid on the susceptibility classification. Of the 14 points, 8 fall within the Very High risk zone, 4 in the High risk zone, and 2 in the Moderate risk zone.

Scale 1:5,000; same CRS and projection as Figure 2. The avalanche sightings symbol represents the white cross markers shown on the map.

RAMMS Simulation of the 2014 Serac Fall

The RAMMS simulation produced a physically coherent reconstruction of the 2014 avalanche. The model log indicates that the simulation terminated due to the time-end condition at 300 seconds, and it is possible that runout distance would extend slightly with a longer simulation window. Key dynamic outputs are summarized below; spatial distributions are shown in Figures 6 through 10.

Flow Height

The simulated maximum flow height reached approximately 35 m in the release and upper transit zone (Figure 6). Through the majority of the flow path, simulated flow thicknesses ranged from 5 to 17.5 m. This is consistent with published estimates for the 2014 event, which described a serac block approximately 35 to 40 m in depth (McMillan, 2014), and with the RAMMS log output that records a maximum flow height of 31.8 m at the final time step. The simulated runout terminus is located near Crampon Point at the base of the Icefall, consistent with eyewitness accounts and the spatial distribution of recovered victims.

Figure 6

RAMMS-simulated maximum flow height for the 2014 serac fall event.

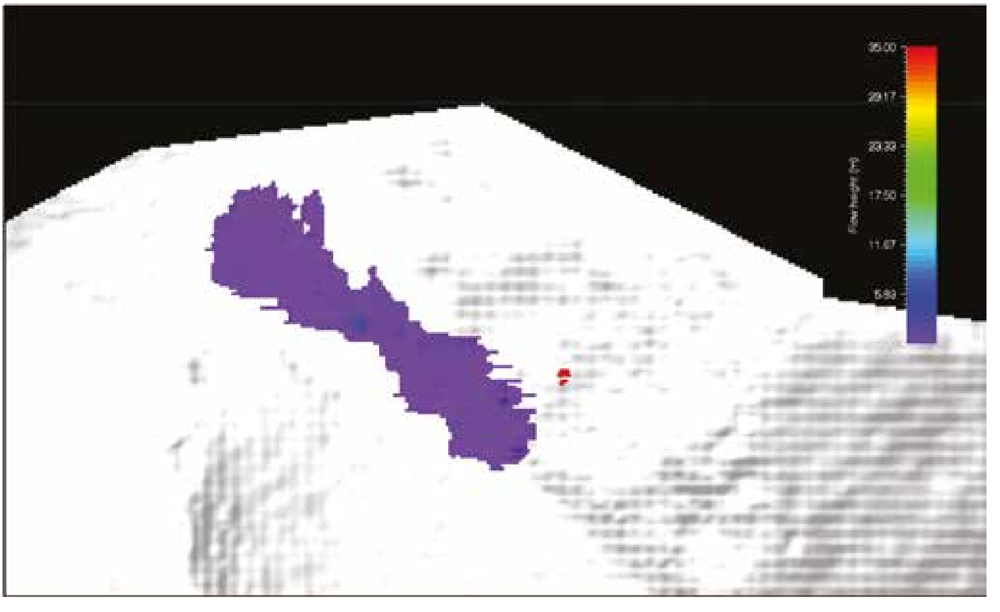

Note: The color scale ranges from near zero (purple) to approximately 35 m (red-orange). The release zone is visible in the upper left. The flow path follows the topographic corridor of the Khumbu Icefall toward Crampon Point at the lower right.

Source: RAMMS output, this study

Flow Velocity

The simulated avalanche reached a peak velocity of 36.2 m/s (approximately 130 km/h) in the steep chutes immediately below the release zone (Figure 7). This value is consistent with the known velocity range for dense-flow ice avalanches on steep glaciated terrain (Gilany &

Iqbal, 2019) and with the order of magnitude expected for a serac of this dimension on slopes of 45 to 55 degrees. Velocities decreased progressively as the flow entered the broader, less confined lower Icefall, stabilizing in the range of 6 to 18 m/s through most of the transit zone. This velocity profile, with rapid acceleration followed by gradual deceleration, is typical of channelled dense-flow events (Christen et al., 2010).

Figure 7

RAMMS-simulated maximum flow velocity for the 2014 serac fall event.

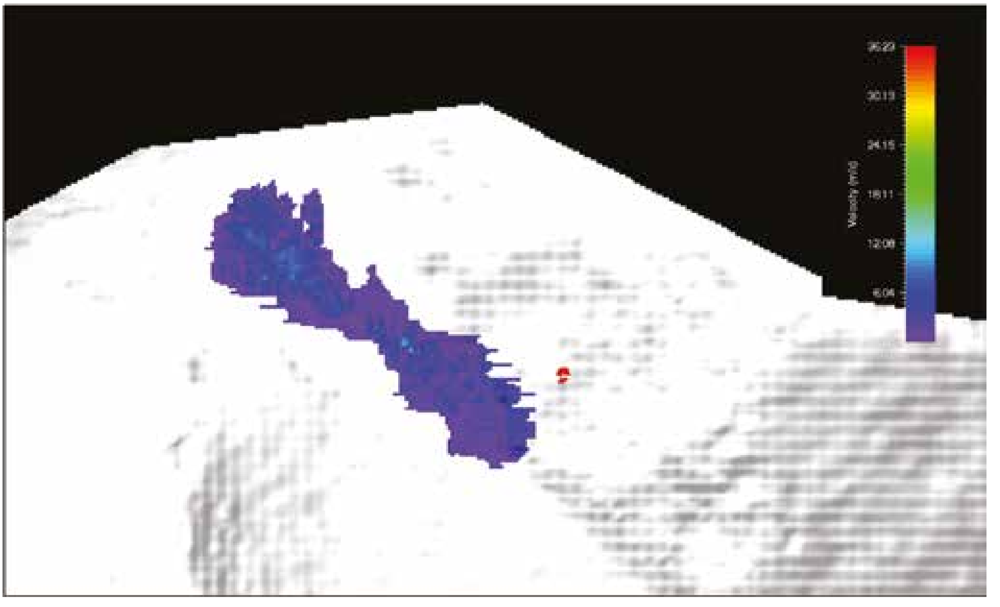

Note: The color scale ranges from near zero (purple/blue) to 36.2 m/s (red). Maximum velocities are concentrated in the steep upper transit zone immediately below the release area.

Source: RAMMS output.

Impact Pressure

Simulated impact pressures reached a maximum of 1,181 kPa (approximately 1.18 MPa) in localized zones where the flow was topographically constrained and accelerating (Figure 8). Pressures in the range of 200 to 600 kPa were distributed across a large proportion of the flow path, indicating a continuously dense, high-momentum mass throughout the transit zone. To contextualize these values, reinforced concrete structures typically fail at pressures of 200 to 1,000 kPa; the simulated pressures at the fatality locations would therefore substantially exceed the resistance of any protective infrastructure or personal equipment. These values are broadly comparable to those reported for the 2012 Gyari serac event in Pakistan, where RAMMS simulations yielded pressures exceeding 2,500 kPa at the highest-impact zones (Gilany & Iqbal, 2019), although the Gyari event involved a considerably larger release volume.

Figure 8

RAMMS-simulated maximum impact pressure for the 2014 serac fall event.

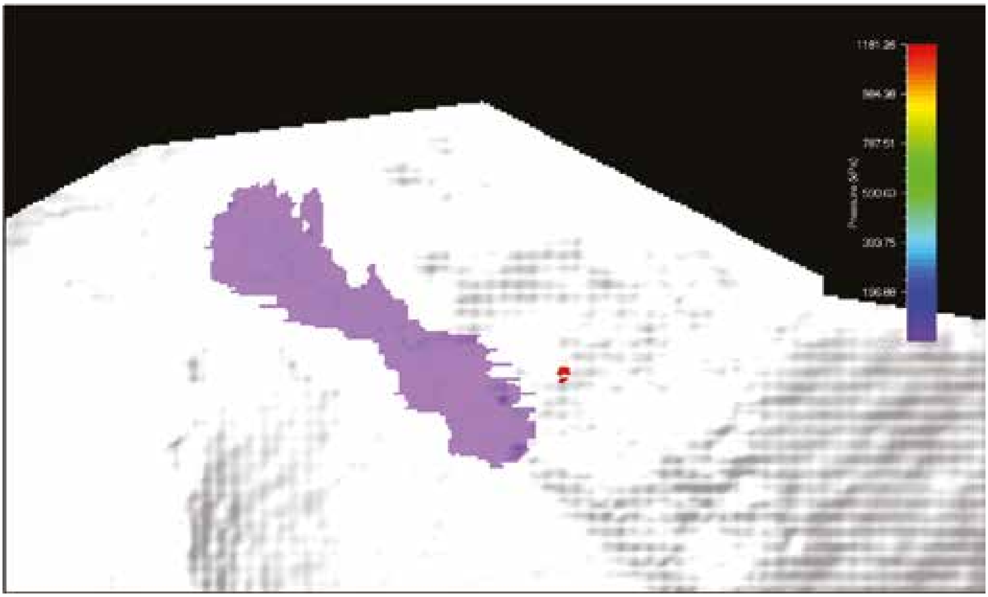

Note: The color scale ranges from near zero (purple) to 1,181 kPa (red). The static visualization represents the spatial maximum across all time steps; peak transient pressures during flow compression are represented by the upper range of the scale.

Source: RAMMS output

Momentum and Shear Stress

Momentum, expressed as mass flux per unit width (m^2 s-1), reached a maximum of 112.8 m^2 s-1 in the upper transit zone and decreased through the lower Icefall, stabilizing in the range of 37.6 to 75.2 m^2 s-1 at the valley floor (Figure 9). This sustained momentum in the lower path indicates that the dense ice mass maintained considerable inertia throughout the runout, consistent with the long transport distance of the debris and the recovery of victims near Crampon Point.

Maximum shear stress reached 60.2 kPa (Figure 10). Shear stress was generally lower in the upper transit zone, where the flow moved rapidly over low-friction glacier ice, and was concentrated at the lower toe of the West Shoulder, where slope angle decreased and the flow decelerated rapidly. This distribution is consistent with a dense-flow or debris avalanche in which basal friction becomes the dominant energy dissipation mechanism during deposition (Christen et al., 2010).

Figure 9

RAMMS-simulated maximum momentum (m^2 s-1) for the 2014 serac fall event.

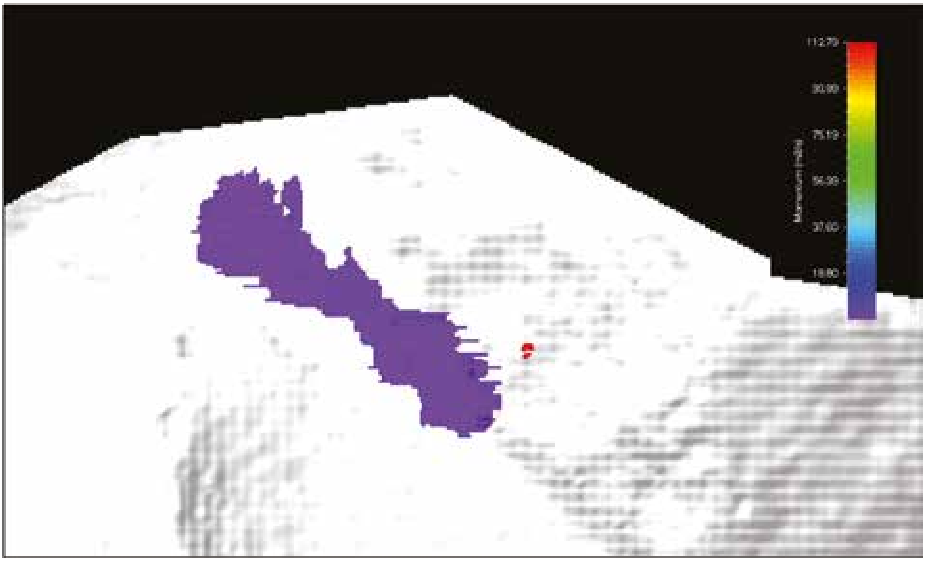

Note: The color scale ranges from near zero (purple) to 112.8 m^2 s-1 (red).

Source: RAMMS output

Figure 10

RAMMS-simulated maximum shear stress (kPa) for the 2014 serac fall event.

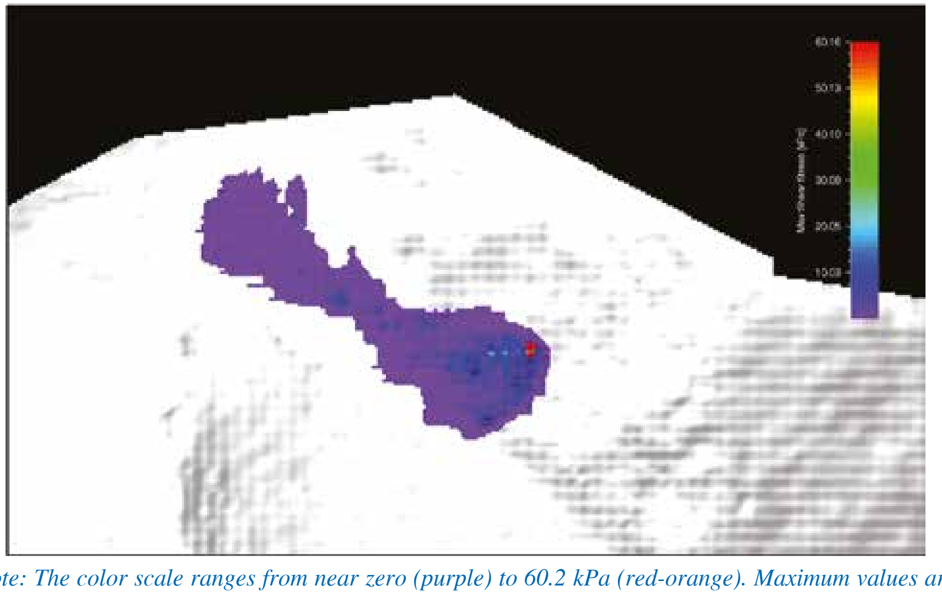

Note: The color scale ranges from near zero (purple) to 60.2 kPa (red-orange). Maximum values are concentrated at the deceleration zone near the base of the West Shoulder.

Source: RAMMS output

Summary of Simulation Outputs

Table 6

Summary of peak RAMMS simulation outputs for the 2014 Everest serac fall event.

Dynamic Parameter	Peak Simulated Value	Location / Interpretation
Release volume (m^3)	23,711	Digitized serac polygon at d0 = 35 m
Maximum flow height (m)	~35	Upper release and transit zone
Maximum velocity (m/s)	36.2	Steep chutes below release zone
Maximum impact pressure (kPa)	1,181	Constrained and channelled sections
Maximum momentum ($m^2\ s^{-1}$)	112.8	Upper descent, West Shoulder
Maximum shear stress (kPa)	60.2	Deceleration zone at Shoulder base

Discussion

Regional Susceptibility and Route Exposure

The susceptibility map confirms quantitatively what the mountaineering community has long recognized empirically: the Khumbu Icefall is among the most avalanche-prone terrain in the Nepal Himalaya. The finding that 34.1% of the study area falls in the High or Very High risk categories is consistent with comparable AHP-based assessments in other Himalayan basins, including the Rishiganga-Raunthigad basin study by Yadav et al. (2023), which reported approximately 47% of the area in these upper categories. The somewhat lower proportion in the present study likely reflects the inclusion of lower-elevation valley terrain in the Upper Dudh Koshi Basin, which contributes substantially to the Very Low and Low risk area.

The concentration of Very High risk terrain along the Khumbu Icefall corridor, through which the standard climbing route must pass, has direct and well-documented safety implications. The temporal pattern of Everest fatalities confirms that the Icefall is the most dangerous section of the ascent (Acharya et al., 2023), and the present map provides a spatially explicit framework within which route modifications or timing adjustments could be evaluated quantitatively. For example, the map could be used to identify the narrowest sections of Very High risk terrain along the route, which are likely to correspond to the highest-priority zones for rapid transit or pre-dawn passage before solar heating destabilizes the snowpack.

Reconstruction of the 2014 Serac Fall

The RAMMS simulation provides a physically coherent reconstruction of the 2014 event. The peak velocity of 36.2 m/s and the maximum flow height of approximately 35 m are consistent with published estimates for this event (McMillan, 2014) and with the velocity ranges reported for dense-flow ice avalanches in comparable glaciated settings (Gilany & Iqbal, 2019; Faillettaz et al., 2016). The simulated maximum pressure of 1,181 kPa substantially exceeds any survivability threshold, consistent with the complete fatality of all individuals caught in the primary flow path.

The spatial correspondence between the simulated runout terminus and the recorded locations of victim recovery near Crampon Point is an important qualitative measure of model performance. The simulation correctly reproduces the general trajectory of the flow southward through the Icefall and the spatial attenuation of velocity and momentum through the lower transit zone. These correspondences provide some confidence in the model's ability to reproduce the broad dynamics of the event, while recognizing that quantitative validation against measured runout distances or deposit thickness is not possible in the absence of systematic post-event field surveys.

Model Uncertainty and Limitations

Several limitations affect the precision and generalizability of the results, and these should be considered when interpreting the outputs. The 12.5 m DEM resolution is the primary constraint on model accuracy. In the Khumbu Icefall, sub-grid terrain features, including individual serac margins and crevasse channels several metres wide, govern flow channelization and dispersion at scales below the model's effective resolution. Higher-resolution topographic data from UAV photogrammetry or repeat LiDAR surveys, currently unavailable for this area, would substantially improve the simulation. For the susceptibility mapping, a higher-resolution DEM would also improve the precision of slope, curvature, and aspect derivation in the steep upper basin.

The absence of in-situ snowpack data represents a further limitation. The RAMMS friction coefficients were calibrated from regional literature rather than from local snow and ice property measurements. Although the calibrated values are consistent with those used in comparable studies, the parameters remain uncertain, and sensitivity analysis (not conducted in the present study) would be a useful addition to future work in this area. Similarly, the WorldClim 2.1 climate layers represent a 1970 to 2000 baseline and do not capture the warming and precipitation changes that have occurred since then, which may affect the correspondence between the mapped climatic susceptibility and current conditions. Given the known warming trend in the Himalaya, actual temperature-related avalanche susceptibility at very high elevations may currently differ from the modeled values.

The expert-based validation, while providing meaningful support for the susceptibility map's broad performance, relies on recall rather than a georeferenced historical inventory. The small sample of mountaineers consulted, and the qualitative nature of their location identifications, mean that this validation should be considered indicative rather than statistically rigorous. The development of a systematic, georeferenced avalanche event database for the Khumbu region would substantially strengthen future validation efforts.

Implications for Hazard Management and Future Research

The integrated GIS-RAMMS framework demonstrated here offers several practical outputs for risk management. The susceptibility map can inform route-setting decisions by identifying the narrowest very high-risk corridors and the terrain features, such as convex ice slopes and north-facing walls, that generate the most frequent avalanche activity. The RAMMS simulation framework can be extended to scenario analysis, for example by varying release volumes or fracture depths to represent worst-case events with return periods of 100 or 300 years, providing a quantitative basis for defining safety exclusion zones around rest stops and equipment caches.

Future research should prioritize several directions. First, the acquisition of very high-resolution topographic data (sub-5 m, preferably from drone or airborne LiDAR) would remove the most significant limitation of both the susceptibility mapping and the RAMMS simulation. Second, the methodology should be extended to other high-traffic mountaineering routes in Nepal, including the Annapurna and Manaslu circuits, toward the development of a nationally consistent avalanche susceptibility framework. Third, integration of climate change projections would allow scenario-based forward modeling of how warming-driven changes in glacier extent, snowpack seasonality, and precipitation intensity may alter the spatial distribution and frequency of avalanche hazard over coming decades. Such forward-looking analysis would be directly relevant to expeditions, mountain communities, and national-level disaster risk management planning in Nepal.

Conclusion

This study produced and evaluated an integrated avalanche hazard assessment for the Upper Dudh Koshi Basin (Everest region, Nepal) by combining GIS-based multi-criteria susceptibility mapping with event-specific RAMMS numerical simulation of the 2014 serac fall. The principal findings are as follows.

The GIS-AHP susceptibility map indicates that approximately 34% of the study area is classified as High or Very High risk, with this hazardous terrain concentrated along the steep glaciated flanks of the major peaks and throughout the Khumbu Icefall corridor. The standard Everest climbing route traverses Very High risk terrain for the entirety of the Khumbu Icefall section. Validation against the 2014 fatality locations, which fall predominantly within the Very High risk zone, and against independent avalanche source identifications by experienced mountaineers (85.7% falling in the two highest risk categories) provides qualitative support for the map's spatial performance.

The RAMMS simulation produced a physically coherent reconstruction of the 2014 event, with a peak velocity of 36.2 m/s, a maximum flow height of approximately 35 m, and localized impact pressures reaching 1,181 kPa. The simulated runout trajectory and terminus correspond broadly with the documented extent of the 2014 avalanche, indicating that the model captures the primary flow dynamics despite the limitations of the available topographic data.

The results demonstrate that the combined GIS-RAMMS approach provides a tractable and informative framework for avalanche hazard assessment in high-mountain environments where field data are sparse and access is restricted. The outputs have direct relevance for expedition operators, route-setting teams, and national authorities responsible for mountaineering safety regulation in Nepal. Improved topographic data, a systematic avalanche inventory, and climate-integrated scenario modeling are identified as the most important directions for advancing this work.

Declarations

Data Availability

The ALOS PALSAR DEM used in this study is available from the Japan Aerospace Exploration Agency. WorldClim 2.1 climate data are available at https://worldclim.org. ESRI Sentinel-2 land cover data are available through the ESRI Living Atlas. RAMMS simulation input files and output rasters will be made available upon reasonable request to the corresponding author.

References

Acharya, A., Steiner, J. F., Walizada, K. M., Ali, S., Zakir, Z. H., Caiserman, A., & Watanabe, T. (2023). Snow and ice avalanches in high mountain Asia: Scientific, local, and indigenous knowledge. *Natural Hazards and Earth System Sciences, 23*(7), 2569-2592. https://doi.org/10.5194/nhess-23-2569-2023

Ballesteros-Canovas, J. A., Trappmann, D., Madrigal-Gonzalez, J., Eckert, N., & Stoffel, M. (2018). Climate warming enhances snow avalanche risk in the Western Himalayas. *Proceedings of the National Academy of Sciences, 115*(13), 3410-3415. https://doi.org/10.1073/pnas.1716913115

Buhler, Y., Kumar, S., Veitinger, J., Christen, M., & Stoffel, A. (2013). Automated identification of potential snow avalanche release areas based on digital elevation models. *Natural Hazards and Earth System Sciences, 13*(5), 1321-1335. https://doi.org/10.5194/nhess-13-1321-2013

Chaulagain, M., Chand, M. B., Pradhananga, D., Dhungana, B., Kayastha, R. B., & Manandhar, S. (2024). Recurring avalanche hazards at Birendra Lake, Manaslu region: Interdisciplinary insights from the April 21, 2024 avalanche event. Unpublished manuscript.

Christen, M., Kowalski, J., & Bartelt, P. (2010). RAMMS: Numerical simulation of dense snow avalanches in three-dimensional terrain. *Cold Regions Science and Technology, 6*3(1-2), 1-14. https://doi.org/10.1016/j.coldregions.2010.04.005

Ciolli, M., Tabarelli, S., & Zatelli, P. (1998). 3D spatial data integration for avalanche risk management. *International Archives of Photogrammetry and Remote Sensing, 32*, 121-127.

Eckert, N., & Giacona, F. (2022). *Towards a holistic paradigm for long-term snow avalanche risk assessment and mitigation. AMBIO, 52*(4), 711-732. https://doi.org/10.1007/s13280-022-01804-1

Faillettaz, J., Funk, M., & Vincent, C. (2015). Avalanching glacier instabilities: Modelling mass release and the dynamics of a break-off event. *Annals of Glaciology, 52*(58), 34-44. https://doi.org/10.3189/172756411799096251

Faillettaz, J., Funk, M., & Vagliasindi, M. (2016). Time forecast of a break-off event from a hanging glacier. *The Cryosphere, 10*(3), 1191-1200. https://doi.org/10.5194/tc-10-1191-2016

Fick, S. E., & Hijmans, R. J. (2017). WorldClim 2: New 1-km spatial resolution climate surfaces for global land areas. *International Journal of Climatology, 37*(12), 4302-4315. https://doi.org/10.1002/joc.5086

Gilany, N., & Iqbal, J. (2019). Simulation of glacial avalanche hazards in Shyok Basin of Upper Indus. *Scientific Reports, 9*, 20077. https://doi.org/10.1038/s41598-019-56523-7

Hao, J., Huang, F., Liu, Y., Amobichukwu, C. A., & Li, L. (2018). Avalanche activity and characteristics of its triggering factors in the western Tianshan Mountains, China. *Journal of Mountain Science, 15*(9), 1897-1411. https://doi.org/10.1007/s11629-018-4941-2

Jenkins, M. (2014). The aftermath of Everest's deadly avalanche. National Geographic Adventure. https://www.nationalgeographic.com/adventure/article/140419-everest-avalanche-sherpas-climbing-aftermath

Kumar, S., Snehmani, Srivastava, P. K., Gore, A., & Singh, M. K. (2016). Fuzzy-frequency ratio model for avalanche susceptibility mapping. *International Journal of Digital Earth, 9*(12), 1168-1184. https://doi.org/10.1080/17538947.2016.1197328

McClung, D., & Schaerer, P. A. (2006). The Avalanche Handbook (3rd ed.). The Mountaineers Books.

McMillan, K. (2014, October 15). Measuring Everest's monster avalanche: How big was the ice block that killed 16 Sherpas? National Geographic News. https://news.nationalgeographic.com/

news/2014/10/141015-everest-sherpa-avalanche-icefall-tragedy-graphic-mountaineering

Mehta, M., & Raina, V. K. (2021). Recent avalanche hazards in the Himalaya: A case study from Mount Everest. *Geological Society of Nepal Journal, 14*(1), 43-57. https://doi.org/10.3126/gsnj.v14i1.38947

Ortner, G., Michel, A., Spieler, M. B., Christen, M., Buhler, Y., Brundl, M., & Bresch, D. N. (2024). A novel approach for bridging the gap between climate change scenarios and avalanche hazard indication mapping. *Cold Regions Science and Technology, 230*, 104355. https://doi.org/10.1016/j.coldregions.2024.104355

Owen, L. A. (2017). Earth surface processes and landscape evolution in the Himalaya: A framework for sustainable development and geohazard mitigation. *Geological Society London Special Publications, 462*(1), 169-188. https://doi.org/10.1144/sp462.9

Saaty, T. L. (1980). The Analytic Hierarchy Process. McGraw-Hill.

Sethia, N., Bhatta, A., & Jain, S. K. (2018). Analytical hierarchy process-based hazard mapping of avalanche-prone areas. *Environmental Earth Sciences, 77*(11), 385. https://doi.org/10.1007/s12665-018-7496-1

Sharma, S., and Ganju, A. (2000). Complexities of avalanche forecasting in Western Himalaya: An overview. *Cold Regions Science and Technology, 31*(2), 95-102. https://doi.org/10.1016/s0165-232x(99)00034-8

Snehmani, Bhardwaj, A., Pandit, A., and Ganju, A. (2014). Demarcation of potential avalanche sites using remote sensing and ground observations: A case study of Gangotri glacier. *Geocarto International, 29*(5), 520-535.

Souckovd, M., Juras, R., Dytrt, K., Moravec, V., Blocher, J. R., & Hanel, M. (2022). What weather variables are important for wet and slab avalanches under a changing climate in a low-altitude mountain range in Czechia? *Natural Hazards and Earth System Sciences, 22*(10), 3501-3525. https://doi.org/10.5194/nhess-22-3501-2022

Strapazzon, G., Schweizer, J., Chiambretti, I., Maeder, M. B., Brugger, H., & Zafren, K. (2021). Effects of climate change on avalanche accidents and survival. *Frontiers in Physiology, 12*. https://doi.org/10.3389/fphys.2021.639433

Thayyen, R. J., Pradhananga, D., & Poudyal, K. N. (2022). Avalanche hazard assessment in the Hindu Kush Himalaya using GIS and simulation models. *Natural Hazards, 101*(2), 823-846. https://doi.org/10.1007/s11069-022-05294-y

Wester, P., Mishra, A., Mukherji, A., & Shrestha, A. B. (Eds.). (2019). The Hindu Kush Himalaya Assessment: Mountains, Climate Change, Sustainability and People. Springer. https://doi.org/10.1007/978-3-319-92288-1

Yadav, P., Pradhananga, D., & Poudyal, K. N. (2023). Remote sensing and GIS-based assessment of avalanching glaciers in the Himalayas. Proceedings of the 14th IOE Graduate Conference.

Yadav, R. R., Negi, P. S., & Singh, J. (2021). Climate change and plant biodiversity in Himalaya, India. *Proceedings of the Indian National Science Academy, 87*(2), 234-259. https://doi.org/10.1007/s43538-021-00034-5

Yanlong, W., & Maohuan, H. (1986). An outline of avalanches in China. *Cold Regions Science and Technology, 13*(1), 11-18. https://doi.org/10.1016/0165-232X(86)90003-0

Yilmaz, B. (2016). Application of GIS-based fuzzy logic and Analytical Hierarchy Process (AHP) to snow avalanche susceptibility mapping, North San Juan, Colorado [Master's thesis]. University of Colorado at Boulder.